RSC Advances

PAPER

View Article Online
View Journal | View Issue



Cite this: *RSC Adv.*, 2025, **15**, 21089

# Investigating laser-induced bond breaking in high-density polyethylene pyrolysis†

Rao Adeel Un Nabi, [ab] Hassan Abbas Khawaja, [c] Yaoxiang Liu,[a] Chaopeng Yang[ab] and Tie-Jun Wang *[ab]

A particular laser harmonic with an effective combination of process parameters can break plastic bonds by surpassing the dissociation threshold. Exploring this direction is imperative to uncover new physics and chemistry related to laser-high-density polyethylene (HDPE) interactions and to understand the phenomena occurring during laser induced degradation. An experiment was conducted in an open-air environment using the first (1064 nm), second (532 nm), and fourth (266 nm) harmonics at a 20 Hz repetition rate, with pulse energies of 5–40 mJ for the first and second harmonics, and 3–10 mJ for the fourth harmonic. The findings revealed that all laser harmonics broke HDPE bonds, with the fourth harmonic being the most effective in directly breaking bonds, particularly C–H bonds, which was evident from a prominent Hα peak at 656.3 nm. The results demonstrate initial, partial, and post-bond breaking, which can address deficiencies in laser-HDPE recycling and enable laser-induced HDPE pyrolysis, which has not been investigated. Optical microscopic analysis showed that craters formed by the fourth harmonic were wider and exhibited more efficient photon absorption with minimal ablation. Additionally, a high confidence interval ($R^2$) value of 0.9758 with increased electron density and plasma temperatures, further supports the efficiency of bond breaking.

Received 26th April 2025
Accepted 28th May 2025

DOI: 10.1039/d5ra02920a

rsc.li/rsc-advances



## 1. Introduction

The main issue regarding the interaction between plastic and laser is the lack of knowledge on the bond's behavior during its breaking down phase.[1,2] LIBS has been frequently utilized, nevertheless, bond dissociation, product route development, and the optimization of process parameters have not been documented.[3,4] This study and previous theoretical insights on laser-induced HDPE pyrolysis, suggest that intense laser treatment could break down polymer bonds. Studies have verified that lasers can break HDPE bonds, but this approach has not yet been employed, further investigation is required to understand this. In recent decades, improvements in this field have involved several machine learning methods, but many advances could be gained by investigating the bond-breaking mechanism.[1]

LIBS is a widely employed atomic emission spectroscopic technique that provides quantitative and qualitative information for elemental analysis. Its rapid analytical performance, minimal destructiveness, and ability to perform standoff detection make it a highly promising technology for diverse applications.[5,6] However, most research has primarily concentrated on identification and classification phases, with limited attention devoted to understanding molecular interactions and disintegration processes. Similarly, pyrolysis, including catalytic, non-catalytic, and microwave techniques, has been used to break down polymers into smaller hydrocarbons, facilitating the extraction of petroleum products for large-scale industrial applications. However, pyrolysis recycling is still inefficient since the input cost exceeds the resulting output value. That is why a hybrid approach combining LIBS and pyrolysis, such as laser-induced pyrolysis, could address the limitations of HDPE recycling and explore the behavior of bonds during degradation and unexplored species formation pathways. Knowledge about the interaction between laser harmonics and HDPE is crucial for understanding bond breaking since this interaction significantly impacts the resultant yield and fundamental physics.[7] Another critical aspect could be determining the minimum energy required to break the bonds inside the plastic, thereby affecting the selection of laser harmonics. Fig. 1(a to c) illustrate that HDPE consists of a large hydrocarbon chain, including C–C and C–H bonds, that require 3.6 eV and 4.2 eV energy, respectively, to be broken.

[a]*State Key Laboratory of High Field Laser Physics, Shanghai Institute of Optics and Fine Mechanics and CAS Center for Excellence in Ultra-intense Laser Science, Chinese Academy of Sciences, Shanghai, 201800, China. E-mail: tiejunwang@siom.ac.cn*

[b]*Center of Materials Science and Optoelectronics Engineering, University of Chinese Academy of Sciences, Beijing 100049, China*

[c]*Department of Automation and Process Engineering, UiT The Arctic University of Norway, 9019, Tromsø, Norway*

† Electronic supplementary information (ESI) available. See DOI: https://doi.org/10.1039/d5ra02920a

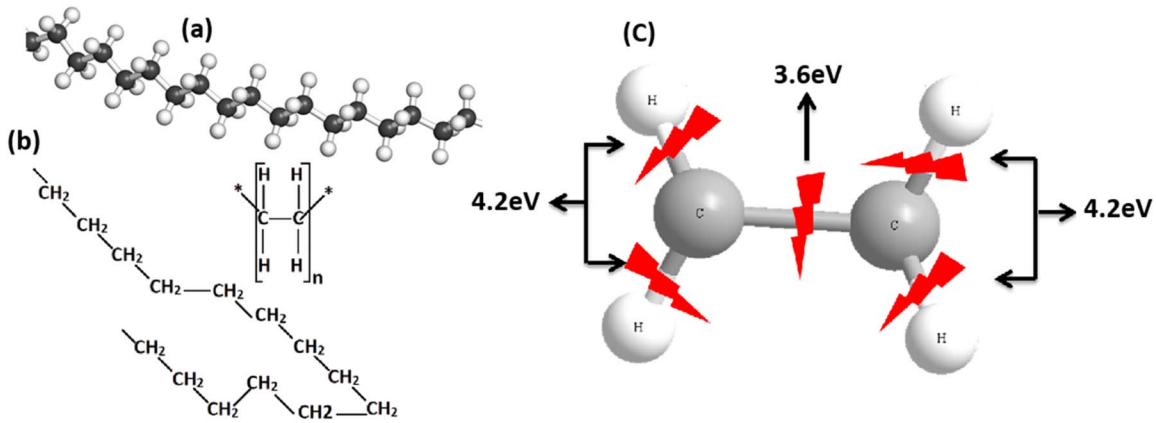


Fig. 1 The molecular structure of HDPE (a) 3D, (b) 2D, and (c) the required threshold to break bonds.

When the photons of different lights interact with the HDPE sample, the atoms in the HDPE absorb energy. Since the behavior of a bond depends on which range of photons it absorbs more readily, the excitation process initiates after the absorption of photons, leading to collisions that can result in breaking. As the atoms absorb energy and transition from the ground to the excited state, this energy is transformed into plasma, leading to various fluorescence emissions. Based on the emitted fluorescence at different wavelengths, it is possible to identify the signals using spectroscopic databases and cited literature. It is important to note that the type of plastic can influence the nature of the obtained spectrum; different types of plastic may behave differently depending on the pulse energy. For instance, instead of increasing the intensity of the spectrum, different pulse energies might produce distinct signal patterns. In the case of HDPE, it has been confirmed that altering the pulse energies could alter the obtained signals – increasing the intensity of the emission spectrum – which also depends on the other process parameters.

Considering the behavior of various laser harmonics, it can be hypothesized that, after breaking the parent C–H and C–C bonds, an Hα peak may be detected, indicating the formation of daughter C–H and C–N bonds due to the fragmentation of the C–C bond. The central question is: where will the Hα originate? It is hypothesized that this peak will most likely arise from breaking the parent C–H bond, as there will be no other plausible source. This is why there should be a focus on investigating Hα rather than C–C, C–N, or C–H bonds. Without clear evidence of how the parent C atoms will react after breaking C–C and C–H bonds, it will be challenging to understand the underlying physics fully. From a hypothetical standpoint, the potential equation in this case could be:

$$[C_2H_4]_n + O_2 + N_2 \xrightarrow{\text{laser harmonics}} C + CN + CO + CO_2 + H_2O + CH + CH_4 + H_2 + \text{others} \quad (1)$$

This above equation can assist in understanding the reason behind not focusing on C fragmentation, since it is nearly impossible to fully understand the actual physics of what happens with C after bond breaking, how C interacts with the environment, to what extent it reacts with elements like N and O, or how it interacts with broken C and H atoms. No simulation, statistical, or numerical approach can provide definitive evidence. As the objective is to conduct laser-induced HDPE pyrolysis, looking more into the chemistry of eqn (1) will only take us so far, however, the analytical debate could aid further. This study will also be conducted in a vacuum to understand the comparable formation routes of Hα as well as other bonds attributed to C since the hypothetical equation could be:

$$[C_2H_4]_n \xrightarrow{\text{laser harmonics}} C + CH + CH_4 + H_2 + \text{other hydrocarbons} \quad (2)$$

In this context, it will be possible to analyze the reaction ratio between parent and daughter C species. Using hypothetical eqn (2), will likely lead to understanding how the parent C reacts and determine the interaction ratios with other fragmentation products. Additionally, it will be intriguing to observe how Hα behaves in a closed environment. The behavior of Hα in a vacuum and insights into the behavior of parent and daughter C, will enhance the understanding of the underlying physics. This information could also be crucial in selecting appropriate gas sensors to detect products formed during laser-induced pyrolysis. Utilizing simulation, statistical methodologies, hypothetical analyses, and potentially including deep learning techniques in this area, will yield positive outcomes for the objective. The possible questions here could be: what about eqn (1) and (2)? Are these initial, intermediate, or final reaction equations? As mentioned above, these are possible hypothetical equations regarding the open and closed environment, but they are not final. Initially, they could be considered intermediate since the HDPE degradation is in the process as a function of experimental conditions. The weight loss indicates that gaseous products are undetectable. Once the vacuum findings have been obtained, eqn (2) could be solved in detail using numerical models.[7,8]

This work aims to examine the previously unexplored interaction between laser and HDPE. The degradation process or product formation involves the behavior of bonds as a function

of a breaking source. This investigation was conducted in an open-air environment to understand more details about laser harmonics and HDPE interactions. Although pyrolysis reactions cannot be performed in open-air due to oxygen and nitrogen, conducting open-air tests offers a more straightforward setup and fewer complications. These tests can still reveal valuable information that helps optimize the conditions for efficient laser-induced pyrolysis. The given study focuses on determining the threshold required to break bonds in HDPE under the influence of different laser harmonics, particularly on C–H bonds. The effects of multiphoton absorption, photodegradation, and the influence of pulse energies as a function of Hα peak intensities, are investigated. This investigation is the first evidence of our hypothetical approach regarding laser-induced HDPE pyrolysis.[1] This study has proven how the bonds can be broken using LIBS under different phenomena.

## 2. Literature review

This section thoroughly examines the limitations associated with LIBS and pyrolysis concerning HDPE recycling. The analysis will elucidate the significance of referenced literature, the shortcomings, and possible alternatives to address the global issue of plastic management in line with the United Nations 2030 Agenda for Climate Change Development and the Paris Agreement. For example, in a recent study on laser–plastic interactions, Junjuri *et al.*[9] proposed a technique called Standoff Identification (SI) using a low-cost LIBS detection system to identify plastic waste in real-time waste management applications, rapidly. Brunnbauer *et al.*[10] argue that targeted 193 nm-LIBS imaging, combined with an intensified charge-coupled device detection system, can detect fluorine-containing small-size polymers, approaching the micrometer scale by monitoring F(I) emissions. Bonifazi *et al.*[11] examined the categorization of black plastic waste using laser-induced fluorescence technology and machine learning algorithms.

Lubongo *et al.*[12] discuss the latest advancements in technology for sorting plastic materials in recycling processes, emphasizing the growing influence of artificial intelligence (AI) and the increasing use of robots in this field. Yang *et al.*[13] provide an overview of recent advancements in using spectroscopic techniques and machine learning to rapidly identify plastic waste, over the past five years. Neo *et al.*[14] developed a polymer spectrum database to enhance chemometric analysis, investigating the impact of hybrid spectroscopic approaches on analysis outcomes. These investigations have demonstrated that LIBS is an effective technique for rapidly handling waste, specifically identifying small-sized polymers. Although LIBS is primarily a diagnostic technique and not intended to break chemical bonds, the laser used in LIBS, under an optimal combination of process parameters, induce bond breaking. However, the exact mechanism remains unreported, possibly due to the complexity involved.

Nevertheless, to effectively address the challenge of large-scale recycling of LIBS and plastic, it is essential to acquire a comprehensive understanding of the plastic degradation mechanism, bond behavior, formation pathways, and the influence of various process parameters and environmental factors. Similarly, in the case of plastic pyrolysis, Shen *et al.*[15] conducted a study to improve the understanding of fluidized bed reactors (FBR) and advance the thermochemical conversion of HDPE through pyrolysis. Their research provides essential experimental and theoretical groundwork for the design of these reactors. Heriyanto *et al.*[16] explored the application of a catalytic mixture in the plastic pyrolysis process to estimate liquid fuel production. Manickavelan *et al.*[17] conducted a study on the pyrolysis of HDPE, using a response surface design to model and analyze the process. Aydogdu *et al.*[18] investigated pyrolysis and hydrogenolysis chemical processes to convert polyolefin plastics into liquid hydrocarbons. The aforementioned recent studies provide evidence that pyrolysis can break down large hydrocarbons into smaller ones and convert them into liquid and gaseous products under various experimental conditions.[19,20]

Moreover, numerical modelling could offer the potential to develop a deeper understanding of the fundamental mechanisms involved in the process. There is a clear need to create a hybrid technique that combines laser and pyrolysis capabilities to address the limitations of plastic recycling. As previously noted, LIBS can provide a detailed analysis of bond behavior, while combining with pyrolysis can offer insight into real-time challenges in plastic recycling.[21,22] Before conducting laser-induced pyrolysis, gathering comprehensive data on the interaction between HDPE and lasers at various harmonics, along with the experimental conditions in closed and open environments currently under investigation, is crucial.

## 3. Description of equipment and experimental configuration

### 3.1. Equipment

To conduct these experiments, it is necessary to establish the following equipment for each setup: the setup includes HDPE samples, two crystals to be installed in the splitter for the second harmonic (532 nm) and the fourth harmonic generation (266 nm), a fused silica focusing lens ($f = 25$ cm) without any additional coating or reflectivity, a rotatable sample holder, a collecting lens ($f = 5$ cm), a neutral density (ND) filter and 532 nm high reflector (HR@532 nm) to control the pump laser intensity of the first and second harmonic respectively, U-link energy meter (SK-10075) to measure the pulse energy, an integrating sphere, air pump, triggering wire, fiber optics (SPLF400-2-UV-P), spectrometer (Ocean Optics HR4000CG UV-NIR) and optical microscope (Olympus BX53M). The comprehensive description of the installation procedure, the logic behind it, precautions, and the significance of each part of the equipment can be found below.

### 3.2. Experimental configuration

A HDPE plastic sheet with a thickness of 0.1 mm was purchased from Ju Jing Rubber & Plastic Products Co., Ltd, China, with a provided a comprehensive datasheet detailing the density (0.94 g $cm^{-3}$), melting point (130–140 °C), tensile strength (23

Table 1 The physical properties of the utilized HDPE sample during our experiments, purchased from Ju Jing Rubber & Plastic Products Co., Ltd, China

| | | | |
|---|---|---|---|
| Density (g $cm^{-3}$) | 0.94 | Shore hardness (D) | 63 |
| Kation index | 900 | Tensile strength (MPa) | 23 |
| Compressive stress at 1% (MPa) | 30 | Elongation at break (%) | 800 |
| Compressive strength (MPa) | 0.01 | Impact strength (kJ $m^{-2}$) | 7 |
| Oxygen index (%) | $10^{10}$ | Notched impact strength (kJ $m^{-2}$) | 0.3 |
| Volume resistivity (Ω cm) | $10^{14}$ | Melting point (°C) | 130–140 |
| Dielectric constant (100 Hz–1 MHz) | 2.4–2.7 | Heat deflection temperature (°C) | 85 |
| Dielectric loss tangent (100 Hz–1 MHz) | 0.001 | Vicat softening point (°C) | 125 |
| Rockwell hardness | R70 | Water absorption (%) | <0.01 |
| Maximum service temperature (°C) | 90 | Minimum service temperature (°C) | −50 |

MPa), and volume resistivity ($10^{14}$ Ω cm) for this material; nevertheless, it is not a Standard Reference Material (SRM). The standards are identical to those employed for HDPE in industrial applications within the fields of science and engineering. A table of all the physical attributes has been reported below in Table 1 which is very similar to pure HDPE. The HDPE sheet was then cut into approximately 3-inch squares for experimental purposes, with a new sample used for each pulse energy interaction. Before laser interaction, the samples were cleaned with alcohol to remove impurities that could generate unwanted signals. Each harmonic required a specific configuration, as shown in Fig. 2(a–c).

The experiments utilized a Dawa-200 pulsed laser, which has four harmonics and can deliver a maximum energy of 200 mJ at the fundamental wave, namely the first harmonic. The laser was pumped directly by a flashlamp powered by the laser power supply. It is crucial to consider the configurations for the first and second harmonics, as they were similar except for the components used to reduce the pump laser intensity, such as the ND filter and HR@532 nm, as demonstrated in Fig. 2(a and b). Fig. 2(c) reflects the setup for the fourth laser harmonic, which was quite different from the first and second harmonic due to the distribution of energy of the laser system; understanding the energy conversion of laser harmonics is essential here since the fundamental laser harmonic has been converted into the second and fourth harmonic. As mentioned above, the total energy of the laser system was 200 mJ, but after installing the laser harmonics, the energy is divided equally, with 50%

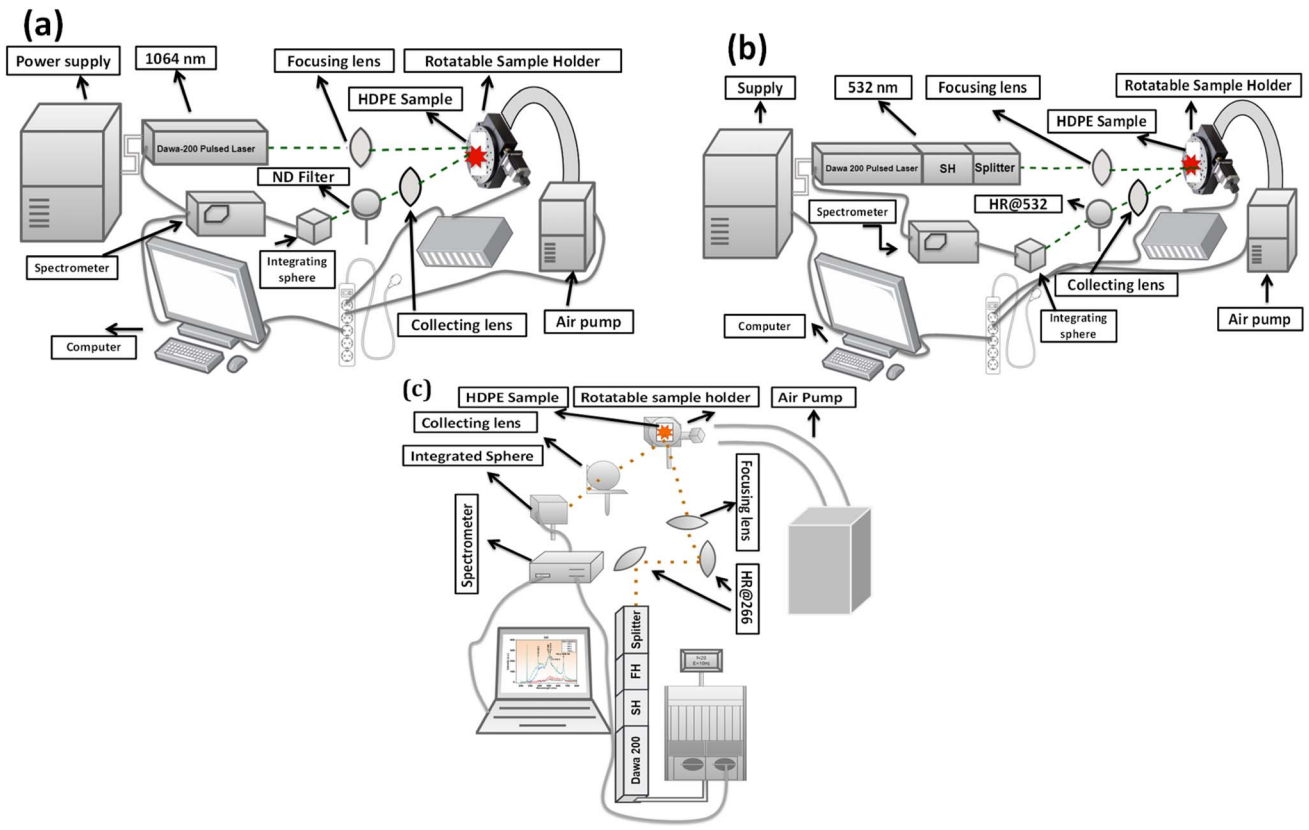


Fig. 2 The experimental configuration for (a) the first harmonic, (b) the second harmonic, and (c) the fourth harmonic.

allocated to each harmonic. This means that upon installing the second laser harmonic, the total energy will be 100 mJ and would be reduced to 18–20 mJ for the fourth harmonic, according to the manufacturer's specifications, which was also confirmed by the data sheet and by measuring the energy using the U-link energy meter. In the case of the fourth harmonic, after installing the high reflectors to attenuate the laser beam, the maximum and stable energy was almost 10–12 mJ; that is why, due to the instrumental limitation, the used stable pulse energy is 3 to 10 mJ.

Due to a slight change in the experimental setup, the illustration for the first harmonic is presented below in Fig. 2(a), while the illustrations for the second and fourth harmonics can be found in Fig. 2(b and c). In the case of the first and second laser harmonic setup, as can be seen below in Fig. 2(a) and (b), a fused silica focusing lens with a focal length of 25 cm and no additional coating or reflection, was positioned in front of the laser output. The laser beam passed through the focusing lens to focus the incoming laser beam onto the HDPE sample. The distance between the focusing lens and the rotating sample holder, which carried the HDPE sample, was 25 cm. This distance matched the lens' focal length, optimizing the interaction between the lens and the HDPE sample. Any deviation from this distance would result in a weak laser–sample interaction. The rotatable sample holder was set at 48 degrees per second to ensure the laser beam did not continually strike the same area, which could ablate the sample and reduce signal quality. After the laser interacted with the HDPE, a collecting lens with a focal length of 5 cm was used to gather the outgoing signals and direct them into the fiber *via* an integrating sphere. The laser-irradiated area on the sample was precisely centered within the lens aperture along the vertical axis to maximize light collection; hence, an integrating sphere was employed instead of a micro-lens to enhance the light entering the fiber. Before the integrating sphere, there were differences in the treatment of the two harmonics. The first harmonic passed through an ND filter, while the second harmonic signals were collected using an HR@532 nm. The ND filter controlled the high intensity of the pump laser in the first harmonic. However, due to concerns about too much high pump laser intensity and to avoid saturation, a reflector was necessary for the second harmonic, as the spectrometer was more sensitive to the wavelength range of 500 nm.

Fig. 2(c) illustrates the conversion of the fundamental laser to the fourth harmonic – the HR@266 nm was positioned at a 45-degree angle in front of the laser head to reflect the fourth harmonic wavelength and block the first and second harmonics. Installing a single HR@266 effectively filtered the first harmonic; however, some remaining influence from the second harmonic wavelength was still not completely filtered out. In order to eliminate the second harmonic, an additional HR@266 was positioned at a 45-degree angle to reflect the fourth harmonic wavelength. Upon installing the additional HR@266, the second harmonic was effectively eliminated. No ND filter or reflector was used before the fiber since the pump laser intensity was controllable. Expecting these factors, the experimental procedure remained the same as that of the first and second harmonics. It involved repeated use of a focusing lens, sample holder, collecting lens, integrating sphere, fiber installation, and signal collection.

The first and second harmonics lasers were tested under identical procedural experimental conditions, which included a repetition rate of 20 Hz, pulse energies of 5 mJ, 10 mJ, 20 mJ, 30 mJ, and 40 mJ, a total of 30 shots, and a microscopic resolution of 3648 pixels. However, the irradiance, reflectance, and absorbance associated with each photon energy differed due to the variation in laser wavelength during the interaction. In the case of the fourth harmonic (266 nm), the energy conversion limitation of the laser system resulted in only one difference in pulse energy: 3 mJ, 5 mJ, 8 mJ, and 10 mJ. The laser triggered the spectrometer. For all cases, the exposure duration of the spectrometer was set to 10 milliseconds (ms) to prevent data collection from a second pulse. Ideally, the exposure time would be 50 ms, calculated from the 20 Hz repetition rate, which is also feasible. However, in the case of a large number of shots in data collection, there will be surface damage, making it challenging to perform microscopic analysis and the possibility of getting more pulse data since the intensity of signals was too strong. Consequently, the exposure duration was decreased to achieve data collection from a single pulse and limit the impact of variations on the error bars. After the laser harmonics ablation, the HDPE samples were further analyzed using an optical microscope to determine the different harmonics' interaction mechanisms. Despite consistency in the focusing setup, equipment arrangement, and data collection throughout each test, the pulse energy of each harmonic varied significantly ranging from 5 to 40 mJ for the 1064 nm and 532 nm harmonics, and from 3 to 20 mJ at 266 nm to investigate the effects associated with varying wavelengths. Each pulse had a duration of approximately 5 ns and was focused to a diameter of 6 millimeters, resulting in estimated irradiances of 0.71 GW $cm^{-2}$ at 1064 nm, 0.35 GW $cm^{-2}$ at 532 nm, and 0.07 GW $cm^{-2}$ at 266 nm, with respective photon energies of 1.17 eV, 2.33 eV, and 4.66 eV. The irradiance values for individual pulse energies can be found in Table 2. These inherent variances influence the interaction between HDPE and the LIBS process, affecting both emission intensity and the disruption of chemical bonds. Additionally, a beam splitter was positioned near the laser head's exit to direct the primary beam onto the crystals required for generating the second and fourth harmonics. The intensity of the laser pulses is dependant upon the reflectance and transmission characteristics of the installed optical components, such as the beam splitter and collecting lens. The details regarding these optical qualities are accessible in the manufacturers' datasheets and were considered during the analysis of the laser's output. In the case of the fourth harmonic, the energy was not stable like the first and second harmonic and a total energy loss of 5 mJ was observed after installing the reflectors or lenses, leaving a maximum of 15 mJ for interaction with the HDPE sample, so it is essential to measure the pulse energy after the reflectors or lenses before approaching the HDPE sample, as there will be a difference in the energy of a pulse from the laser head and the sample being targeted. Another aspect to consider is installing an air pump on the upper part of

the HDPE sample holder since cyanide was emitted during the interaction due to the reaction between broken carbon and the surrounding environment. To ensure safety during these experiments, extra precautions such as wearing goggles, a mask, and gloves were taken to prevent potential hazards.

## 4. Results and discussion

### 4.1. Results

To understand the obtained spectrum, it is essential to know how various laser harmonics interact with HDPE. The threshold energies to break C–C and C–H bonds were 3.6 eV and 4.2 eV, respectively. The photon energies for the first, second, and fourth harmonics were 1.17 eV, 2.34 eV, and 4.6 eV, with corresponding pulse energies of 10 mJ, 5 mJ, and 3 mJ; below these thresholds, there is no observed interaction signal with HDPE. Two significant phenomena occur when HDPE is exposed to different laser harmonics: photothermal and photochemical effects. The photothermal effect involves absorbing photons, generating heat, and inducing thermal degradation due to abundant absorbed photons. The photochemical effect entails exciting and breaking bonds. HDPE absorbs light from infrared (IR), visible, and UV ranges, leading to heat buildup, thermal degradation, and excitation, forming free radicals. Notably, the fourth harmonic (UV region) directly breaks bonds due to enough photon energy, and multiphoton absorption leads to the photothermal phenomenon of generating heat and radicals. These radicals initiate reactions, releasing fluorescence at different wavelengths as a function of pulse energies. It is now easier to understand the findings revealed by the interaction of varying laser harmonics. In this context, it is essential to recall

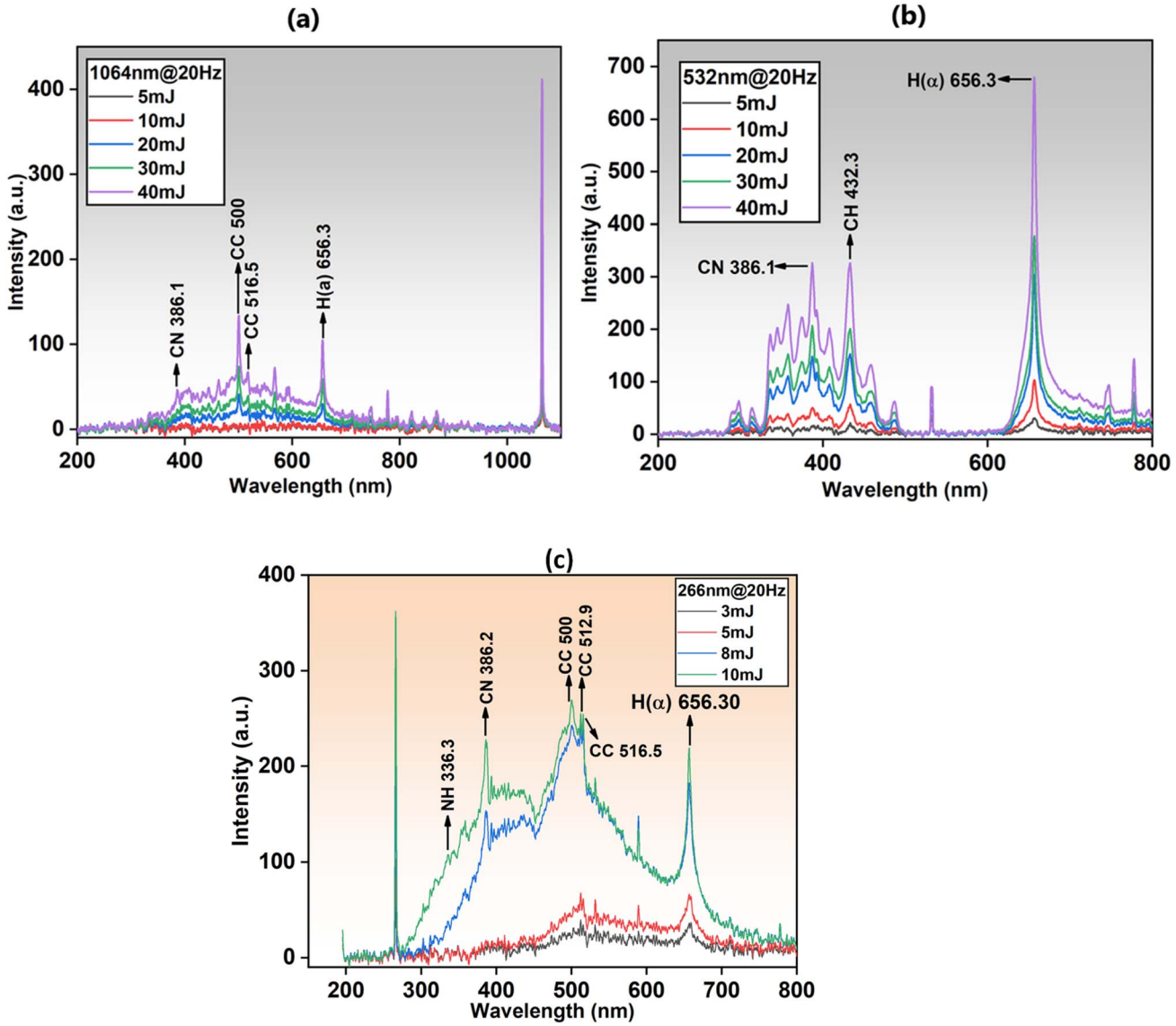


Fig. 3 The HDPE response spectra with (a) the first harmonic, (b) the second harmonic, and (c) the fourth harmonic. In the case of the second harmonic, the absence of CC emission at these wavelengths was attributed to the HR@532 filter installation.

the objective to explore laser-induced HDPE pyrolysis. Fig. 3(a–c) reveals the spectra of three laser harmonics with HDPE.

After the breaking of C–C and C–H bonds, the unpaired electrons of carbon (C), hydrogen (H), and nitrogen (N) atoms interact with other broken C, H, and N atoms. This interaction results in light emission at specific wavelengths, known as fluorescence. The wavelengths at which fluorescence occurs were as follows: C–C at 500 nm, C–C at 516.5 nm, C–H at 432.3 nm, C–N at 386.1 nm, and H(α) at 656.3 nm.[23,24] The fluorescence intensity was dependent on the energy of the pulse, as illustrated in Fig. 3 (a–c). The increased intensity of these peaks in all harmonics suggests that the fourth harmonic was more proficient in bond cleavage since its photon energy is higher, efficiently initiating the degradation process, as seen in Fig. 3(c). It is crucial to comprehend the process underlying these emissions lines. For instance, the emission of C–N at a wavelength of 386.2 nm occurs due to the cleavage of parent C–H bonds, enabling the carbon to react chemically with N in the surrounding environment.[25] The high reactivity of N and the superior bonding stability of C allow the production of cyanide (C–N).

The reaction between hydrogen (H) from the parent C–H bond and nitrogen (N) to form an N–H bond is theoretically possible. However, bond formation requires stability, which may be inhibited by factors such as high-energy collisions of free radicals, plasma formation, and multiphoton-induced thermal effects. This effect is evident in Fig. 3(c), where the N–H signal at 336 nm appears with significantly lower intensity than the prominent C–N bond. These conditions increase the likelihood of C forming a stable bond with nitrogen rather than hydrogen. The spectrum shown in Fig. 3(c) displays a continuous background within the fluorescence wavelength region, along with identifiable C–C and C–H emissions. The generation of plasma, combined with enhanced ionization and limited availability of free electrons, contributes to a broadened spectrum and an increase in continuum intensity through Bremsstrahlung radiation. While the time-delay optimization appears promising for suppressing the continuum and improving spectral line resolution, this study did not employ gating or time-delay mechanisms. Although there remains a possibility that hydrogen from broken C–H bonds could react with nitrogen, establishing definitive conclusions without empirical proof is challenging due to the inherent bond stability of carbon. The emission signals at 500 nm, 512.9 nm, and 516.5 nm correspond to C–C bonds and result from the cleavage of parent C–C bonds, followed by interactions with C radicals.[26] A critical consideration is whether these emission lines originate from the parent C–C bond free radicals or carbon released due to the breakdown of C–H bonds. While this question presents an avenue for further exploration, the current experimental approach does not provide sufficient means to determine whether these emissions primarily result from original C–H bonds or subsequent interactions involving daughter C–C bonds. The Hα emission, detected at a wavelength of 656.3 nm, belongs to the Balmer series and is commonly observed in organic materials such as plastics. In this study, the Hα signal was attributed to the cleavage of C–H bonds, as no other significant sources were identified, as shown in Fig. 3(a–c). The primary objective of this investigation is to demonstrate the cleavage of C–H bonds using the fourth harmonic of the laser. It should be noted that the laser-induced plasma formation might involve nearby gases, such as ambient hydrogen, potentially influencing the measured Hα signal. To confirm the origin of the Hα emission line at 656.3 nm observed during laser-induced breakdown, control experiments were performed under identical conditions with and without the presence of the HDPE sample. These trials were repeated several times to validate the results. It was observed that no significant Hα emission appeared in the spectra when the laser interacted with air alone, without the HDPE sample. This strongly suggests that the hydrogen emission originates from the HDPE itself, not from atmospheric hydrogen. A representative spectral image from the air breakdown condition (without HDPE) is provided in the ESI† file to support this observation. However, a control condition in which the laser beam was directed into the air, excluding the HDPE, was used to verify the source of Hα emission. The spectrometer did not identify any Hα emission signals during the control experiment under identical procedural conditions, confirming that the Hα emissions in the primary investigation originate from the HDPE. The analytical procedure is influenced by external conditions that might modify the plasma's chemical composition and impact background signals. The emission peaks suggest that HDPE experiences laser-induced dissociation, which could be attributable to the ratio of C–H bonds surpassing C–C bonds by a factor of two. A more rigorous control, such as doing studies in an inert environment (*e.g.*, argon or nitrogen), would yield further evidence that the Hα emission is exclusively derived from the C–H bonds of HDPE. The subsequent inquiry will be carried out in a vacuum to obtain clearer information. The dependability of analysis and diagnostic accuracy will improve due to these advancements in spectrum interpretation approaches.

Emphasis on the Hα signal stems from two main factors. First, it is essential to consider the study's primary objective, which involves laser-induced pyrolysis. Conducting this process in an uncontrolled environment presents challenges, yet the data obtained and comparative findings under identical procedural experimental conditions in a vacuum, will contribute to a more comprehensive analysis. Examining emissions from C–C and C–N bonds in excessive detail may divert focus from the core objectives and be considered extraneous. Following the breaking of C–C bonds and the release of carbon from C–H bonds, C–C bonds readily undergo reactions with other C–C bonds and free radicals, including nitrogen.[27] Since the experiment was conducted in an open-air environment, CN emissions were excluded from the analysis, as atmospheric nitrogen could readily influence these signals. Prioritizing the avoidance of C–C emissions was a logical approach due to the potential for carbon to react with C–C bonds and free radicals. Carbon can participate in degradation processes leading to the formation of compounds such as C–O or $CO_2$.[28] These emissions were not considered significant to the study without solid experimental evidence supporting their relevance. In contrast, the Hα emission is directly linked to the

cleavage of C–H bonds, a finding that has been empirically confirmed, making it the primary focus of this research. Considering the potential interaction of nitrogen (N) with both carbon (C) and hydrogen (H) released from broken C–H bonds, it is theoretically possible for N to react with H. However, due to the higher electronegativity of N, it has a greater tendency to bond with C rather than H, forming a stable C–N bond. This observation is supported by experimental evidence.

Additionally, for the fourth harmonic, the fluorescence wavelength region associated with C–C and C–H emissions exhibits a continuous spectrum, as observed in Fig. 3(c). This phenomenon is typically attributed to increased plasma formation, higher ionization levels, and a reduction in the abundance of free electrons. A key observation in this study is that increasing pulse energy leads to enhanced C–H bond cleavage, as evidenced by the rise in Hα line intensity. Experimental confirmation demonstrated that hydrogen molecules in the air did not influence the Hα signal. This was validated by conducting laser harmonic tests in air without the HDPE sample, during which no H signals were detected. Consequently, the Hα signal is exclusively associated with the cleavage of C–H bonds. The absence of fluorescence emission in the 500–580 nm range was attributed to the installation of the HR@532 filter since the excessively high intensity of the pump laser, which could not be fully controlled using the ND filter, and the high sensitivity of the spectrometer within this wavelength range, lead to potential saturation. This was confirmed through tests in which the ND filter was applied to reduce the pump laser intensity, causing all other emission lines to disappear. These findings suggest that the pump laser intensity, regulated by the HR@532 filter, was the primary reason for the absence of emission lines in this range.

Additionally, separate views for the C–C lines at 500 nm and 516.5 nm and the Hα line at 656.3 nm can be seen in Fig. 4(a to c), illustrating the pulse energy dependency on each harmonic. Fig. 4(a–c) show that spectral intensity grows more substantial and more pronounced with increasing pulse energy. For all harmonics, higher pulse energy corresponds to higher bond breaking. The emitted signals reveal a steady increase in bond breakage as pulse energy rises from 5 mJ to 10 mJ for the first and second harmonics and from 3 mJ to 5 mJ for the fourth harmonic. At elevated pulse energies ranging from 20 mJ to 40 mJ for the first and second harmonics and from 8 mJ to 10 mJ for the fourth harmonic, the rate of bond breakdown increases markedly. This phenomenon in the first and second harmonics is likely due to multiphoton absorption. In the case of the fourth harmonic, the presence of high-energy photons, increased excitation levels, more significant heat generation, and intensified collisions between free radicals, contribute to this effect.[29] According to Fig. 3, the emission intensity at 532 nm excitation is significantly higher than that at 1064 nm excitation, despite both receiving identical pulse energy. This is because the photon energy at 532 nm (2.33 eV) facilitates more efficient energy transfer to HDPE, resulting in increased absorption and reduced reflection compared to 1064 nm (1.17 eV). The decreased intensity observed at 266 nm, in contrast to the other laser harmonics, is primarily due to challenges in generating the fourth harmonic within the instrument. The energy produced at 266 nm was limited to 3–10 mJ due to the system's low conversion efficiency. Furthermore, increased beam divergence, potential scattering, and the influence of plasma shielding at this shorter wavelength may further reduce the emission intensity. The operated laser was directly triggered by the spectrometer, and spectral data were acquired automatically

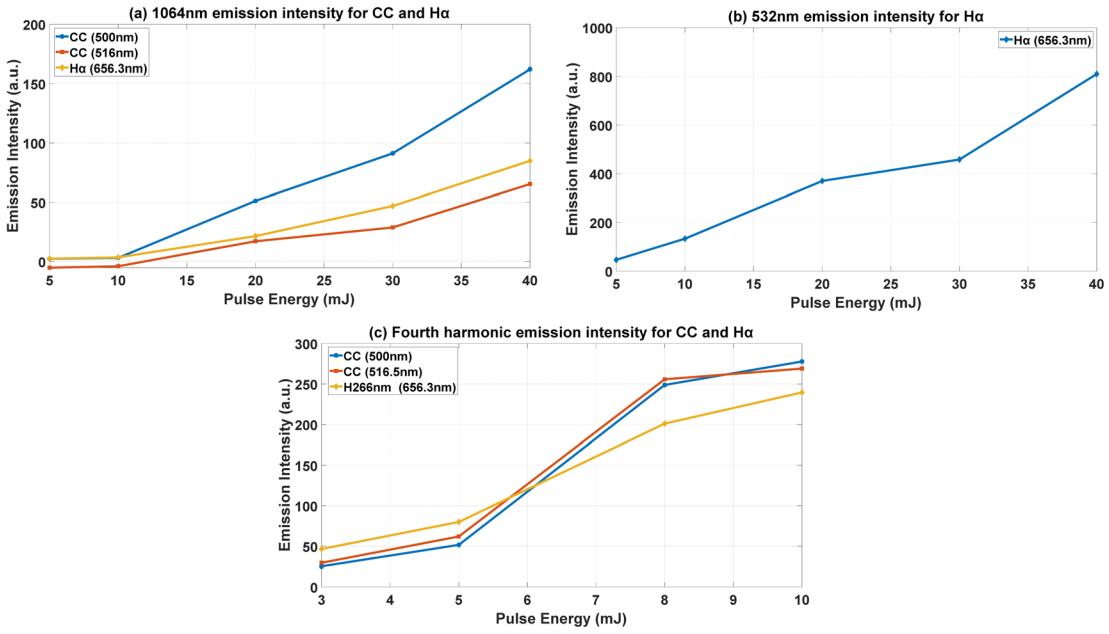


Fig. 4 The emission intensity of CC and Hα as a function of pulse energy for (a) the first harmonic, (b) the second harmonic, and (c) the fourth harmonic.

*via* a designated software program. As a result, the spectral range acquired for each harmonic was automatically adjusted based on the signal strength and the duration of the measurement interval, since the laser was directly triggered by the spectrometer. The variation in spectral windows shown in Fig. 3 across the harmonics is attributed to this synchronized and signal-dependent method of data collection. After breaking the C–C and C–H bonds, some gaseous product formation has not yet been directly identified, depending on the intensity of pulse energy, number of shots, and laser ablation time. In the case of the first and fourth laser harmonic, even at higher pulse energies such as 40 mJ and 10 mJ, no significant weight loss was found after 30 laser shots and a 1.5-second laser ablation time; however, it is believed that a chemical interaction occurred between N and C, resulting in a slight decrease in weight/mass loss. The mass loss calculations were performed using an OHAUS analytical balance with manufacturer specifications of 1 mg readability, ±1 mg repeatability, and ±2 mg linearity, as seen in Fig. 12 in the ESI.† The balance was calibrated before each measurement, and a draft shield was used to minimize air-related environmental effects. In the experiment, the sample's mass before ablation was 4.5753 g, and after ablation, it was 4.5750 g, resulting in a mass difference of 0.3 mg, corresponding to a 0.0066% loss. The measured mass loss was within the balance's specified readability and repeatability range of ±1 mg. However, multiple replicate measurements were not conducted. Determining whether the slight mass variation observed originates from laser ablation effects or instrumental fluctuations is difficult. This study primarily focused on the spectral behaviour of laser-HDPE interactions rather than directly measuring open-air mass loss. Future weight loss evaluations will be included in vacuum experiments to provide more accurate data, which should promote laser-induced HDPE pyrolysis. However, it is possible to understand this curiosity by employing higher pulse energy, ablation time, and a suitable sample holder to hit the new spot every time, which could lead to the maximum sample weight loss.[30]

Theoretically, laser harmonic interaction with HDPE begins a two-stage process that results in bond fragmentation and product formation. The first stage of HDPE interaction with photon energy through direct impact and multiphoton absorption leads to ionization rather than direct bond breaking while producing a hot plasma consisting of atomic C and H species along with ionic $C^+$ and $H^+$ species.[31] The cooling plasma allows the species to combine into radicals, including $CH_3^{\bullet}$, $C_2H_5^{\bullet}$, and $H^{\bullet}$. These radicals could initiate additional chemical reactions by abstracting hydrogen atoms or undergoing recombination, which could provide gaseous products, as depicted in Fig. 5. However, the actual final primary and by-products depend on different factors. As no literature has been reported on laser-induced reaction mechanisms, it is hard to make any solid decision. Further investigation will provide insight into the final products.

The breaking of HDPE bonds was found to be laser wavelength-dependent, which can also be influenced by the absorbance and reflectance of HDPE, as reported below based on the corresponding photon energies. However, the actual phenomena of absorbance and reflectance of different photon energies by HDPE may vary depending on the experimental conditions. The interaction between laser and HDPE was significantly influenced by the wavelength, resulting in significant variations in both irradiance and the material's optical characteristics which depends on the process parameters in terms of laser–HDPE interaction.[32,33] The fourth harmonic (266 nm) laser could deliver higher photon energy and significant surface absorption, even with lower pulse energy ranges of 3–10 mJ. Enhanced ablation efficiency on the surface is noted, accompanied by intensified LIBS emission in the Hα line at 656.3 nm. The absorption of the second harmonic (532 nm) is moderate (60–70%) and results in significant plasma emission.

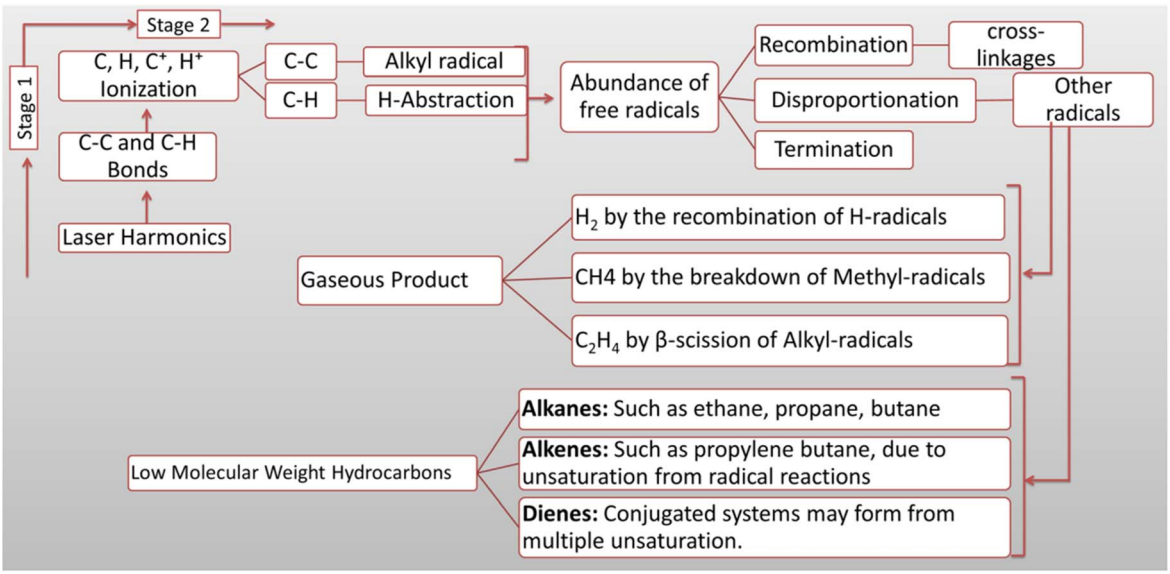


Fig. 5 The hypothetical laser-induced HDPE pyrolysis products.

Table 2 The corresponding laser irradiance, HDPE properties, and fundamental process parameters for each harmonic

| Process parameters | Calculations |
|---|---|
| Pulse duration | 5 ns |
| Laser spot | 6 mm |
| Spot area calculation | $\Pi r^2$ |
| Peak power per pulse | $P = \frac{\text{Pulse Energy}}{\text{Pulse Duration}}$ |
| Irradiance calculation | $I = \frac{\text{Peak Power}}{\text{Spot area}}$ |

The calculated irradiance and approximated reflectance and absorbance[32,33]

| Laser wavelength (nm) | Pulse Energy (mJ) | Irradiance (W cm$^{-2}$) | HDPE reflectance (%) | HDPE absorbance (%) |
|---|---|---|---|---|
| 1064 (first) | 5 | $3.53 \times 10^6$ | ~40–50 | ~50–60 |
| | 10 | $7.07 \times 10^6$ | | |
| | 20 | $1.41 \times 10^7$ | | |
| | 30 | $2.12 \times 10^7$ | | |
| | 40 | $2.83 \times 10^7$ | | |
| 532 (second) | 5 | $3.53 \times 10^6$ | ~30–40 | ~60–70 |
| | 10 | $7.07 \times 10^6$ | | |
| | 20 | $1.41 \times 10^7$ | | |
| | 30 | $2.12 \times 10^7$ | | |
| | 40 | $2.83 \times 10^7$ | | |
| 266 (fourth) | 3 | $2.12 \times 10^6$ | ~10–20 | ~80–90 |
| | 5 | $3.53 \times 10^6$ | | |
| | 8 | $5.65 \times 10^6$ | | |
| | 10 | $7.07 \times 10^6$ | | |

The primary infrared laser (1064 nm), with energy levels up to 40 mJ, exhibits limited absorption and elevated reflection, hence diminishing the LIBS signal and reducing the effectiveness of surface coupling. Fig. 3(a–c) illustrate that enhanced laser–sample interaction and absorption result in increased LIBS emission intensities. Table 2 presents the values of corresponding laser irradiance and HDPE optical properties for each harmonic.

### 4.2. Significance of numerical models

Fig. 6(a to c) demonstrates the relation between the Hα intensity and the pulse energy during C–H bond breaking. According to the slope equation $y = mx + c$, eqn (3)–(5) are the Hα emission for the first, second, and fourth laser harmonic:

$$\text{First Harmonic: } Y = 3.892x - 19.2 \quad (3)$$

$$\text{Second Harmonic: } Y = 20.673x - 72.53 \quad (4)$$

$$\text{Fourth Harmonic: } Y = 29.57x - 52.37 \quad (5)$$

Here, $y$ (dependent variable) denotes the Hα intensity, while $x$ (independent variable) represents the pulse energy. The slopes 3.892, 20.673, and 29.57 indicate that for every unit increase in pulse energy, Hα intensity increases proportionally for the first, second, and fourth harmonics, respectively. This confirms a linear relationship between the HDPE sample's emission intensity and pulse energy.[34] The 19.2, 72.53, and 52.37 intercepts represent the theoretical Hα intensity at zero pulse energy. Negative or near-zero intercepts are expected, as emission does not occur without sufficient excitation energy identified at a minimum of 3 mJ. The $R^2$ values of 0.96, 0.96, and 0.97 for the respective harmonics indicate that the linear model explains 96 to 98% of the variation in intensity, suggesting minimal influence from noise or instrumental error.[35] Scientifically, the linear trend and high $R^2$ demonstrate an efficient and consistent energy absorption mechanism in HDPE, particularly under 266 nm irradiation.[36] The slight deviation of $R^2$ from 1.0 likely

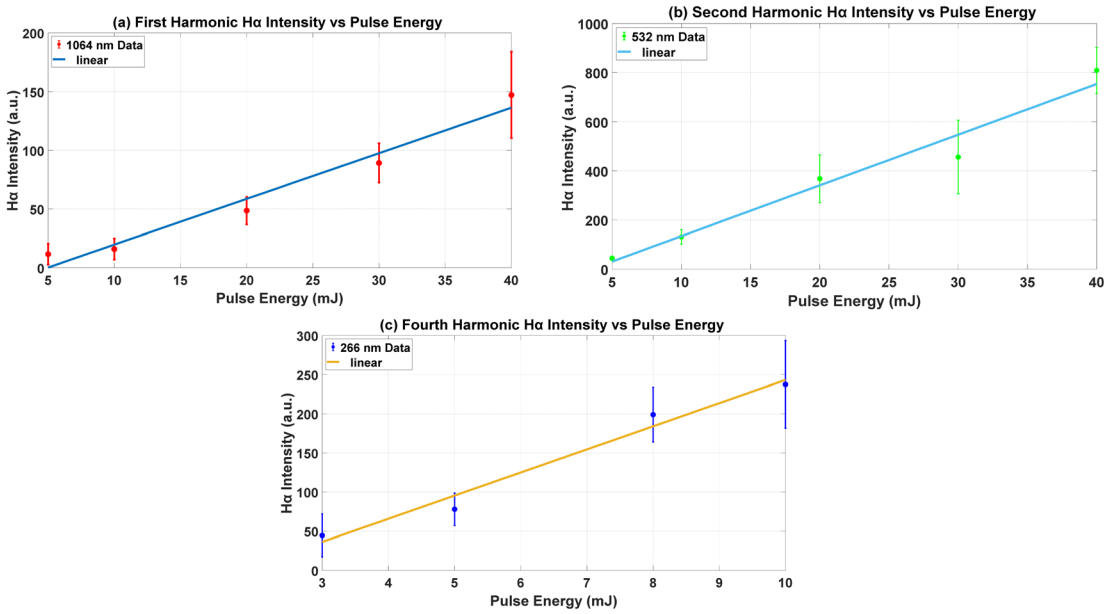


Fig. 6 The comparison of Hα intensity with error bars and linear fit for (a) the first harmonic, (b) the second harmonic, and (c) the fourth harmonic.

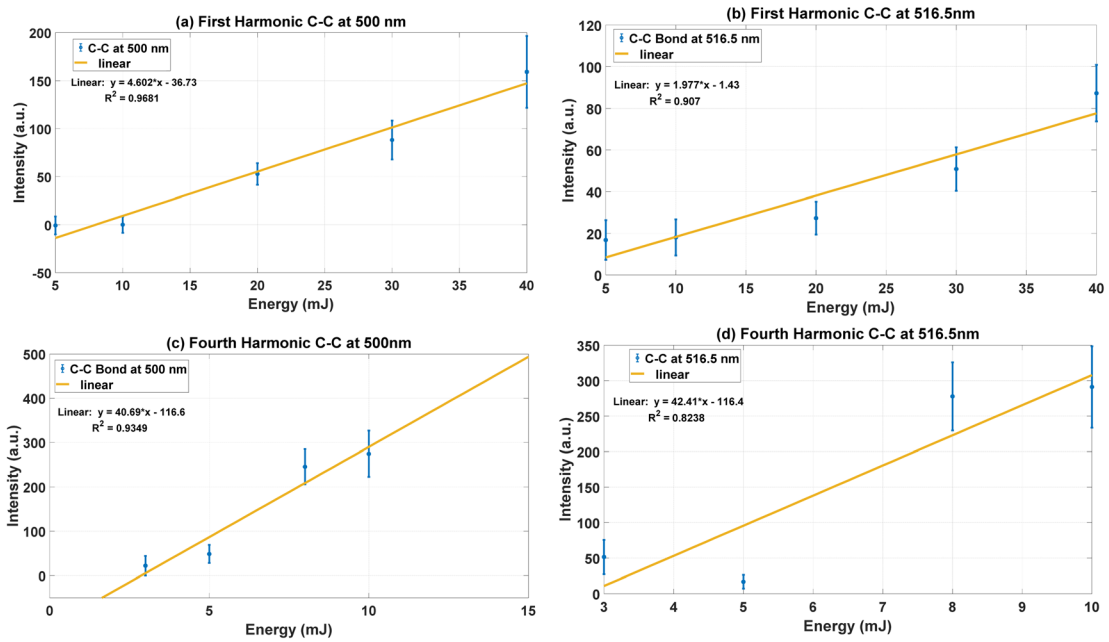


Fig. 7 C–C breaking at an emission intensity of 500 nm and 516.5 nm for the first harmonic ((a) and (b)) and the fourth harmonic ((c) and (d)).

results from minor experimental fluctuations, but does not undermine the model's reliability. Further confirmation of C–C bond breaking across all laser harmonics along with corresponding slope equations, model significance, and linear fit is presented in Fig. 7(a–d), which reflects that the C–C bonds have also been broken and emit the intensity at different emission wavelengths. However, in this study, the C–C breaking is not the primary goal due to the interference of an open environment.

The Hα emission intensity depends on the rate at which C–H bonds dissociate because the Hα line emits light from released atomic hydrogen at wavelength 656.3 nm. All laser harmonics were operated in an open environment without a sample, which showed no Hα signal was present at this time. It confirms that the Hα emission only comes from C–H bond dissociation. The harmonic excitation conditions produced Hα peaks, but their intensity levels differed substantially from each other. The Hα signal intensity from C–H bond dissociation by photons was strongest at the fourth harmonic because its photon energy (4.66 eV) exceeded the C–H bond dissociation energy (~4.3 eV). The emission intensity was reduced when using the lower photon harmonics (1064 nm and 532 nm) relative to the fourth harmonic (266 nm). This signal was only observed within the plasma plume, which is solely possible when C–H has been broken and produces emission intensity at 656.3, so it is scientifically reasonable to link the Hα intensity with C–H breaking.

### 4.3. Determination and comparison of laser-induced plasma parameters

This study examined plasma temperature using the Boltzmann plot method, a conventional technique for LIBS diagnostics to determine temperatures based on LTE assumptions.[37] The analysis used a modified expression based on the Boltzmann distribution, as shown in eqn (7). The investigation of atomic emission lines excluded the computation of solid angle ($\Omega$) due to the observations being conducted with a fixed detector configuration. The constant $\Omega$ value does not affect the relative intensity or the resultant plasma measurements, acting as a universal scaling constant. The modified form acted as a temperature estimate source by analyzing the Hα emission line at 656.3 nm, which was derived from line intensity and Boltzmann expression since it is frequently employed to examine the dynamics of the hydrogen-rich plasma. Examining ultra-fine rotational structures in molecular band emission may assist in determining plasma temperatures generated by short wavelengths, such as the fourth harmonic. The foundational mathematical connection derived from the exponential intensity-energy dependency resulted in this formulation, which incorporates the electron density $N_e$ absent in conventional LIBS Boltzmann illustrations, as shown in eqn (6). The conventional linearised Boltzmann relation was employed for temperature assessment due to its alignment with LIBS methodologies and capacity to provide consistent findings. The detailed information is presented in Table 3, Fig. 8(a and b). The Hα emission line (656.3 nm) was used to determine the plasma temperature accurately, particularly for hydrogen-rich plasma diagnostics. Additionally, the plasma generated by the fourth harmonic exhibited distinct atomic emission lines, with Hα being the most prominent. The use of the Hα line offers several advantages due to its minimal spectral interference. However, ultra-fine rotational structures can also facilitate the determination of plasma temperature for shorter wavelengths, such as the fourth harmonic. The electron density was calculated from Stark broadening using the relation $\Delta\lambda_{1/2} = 2 \times 10^{-8} N_e^{2/3}$.[38,39]

Table 3 The calculated plasma temperature and electron density as a function of pulse energy and Hα spectral emission

| Laser harmonics (nm) | Pulse energy (mJ) | Hα intensity (a.u.) | Plasma temperature (K) | Electron density ($cm^{-3}$) |
|---|---|---|---|---|
| First harmonic (1064) | 5 | 2.470 | 2737.34 | $1.0 \times 10^{17}$ |
| | 10 | 3.581 | 2742.11 | $1.0 \times 10^{17}$ |
| | 20 | 21.481 | 2762.18 | $1.2 \times 10^{17}$ |
| | 30 | 46.902 | 2771.95 | $1.3 \times 10^{17}$ |
| | 40 | 84.877 | 2789.21 | $1.4 \times 10^{17}$ |
| Second harmonic (532) | 5 | 46.097 | 2730.67 | $9.0 \times 10^{16}$ |
| | 10 | 133.242 | 2745.22 | $1.0 \times 10^{17}$ |
| | 20 | 369.836 | 2785.56 | $1.1 \times 10^{17}$ |
| | 30 | 458.245 | 2800.45 | $1.2 \times 10^{17}$ |
| | 40 | 810.544 | 2885.34 | $1.3 \times 10^{17}$ |
| Fourth harmonic (266) | 3 | 46.569 | 2655.34 | $8.0 \times 10^{16}$ |
| | 5 | 79.946 | 2700.56 | $8.5 \times 10^{16}$ |
| | 8 | 201.054 | 2780.45 | $9.0 \times 10^{16}$ |
| | 10 | 239.636 | 2850.34 | $9.5 \times 10^{16}$ |

$$\frac{I_\lambda}{g_u N_e A_{ul} \Delta E} \propto \exp\left(-\frac{E_u}{k_B T}\right) \quad (6)$$

$$T = \frac{E_u}{k_B}\left[\ln\left(\frac{A_{ul}\, g_u N_e}{I_\lambda}\right)\right]^{-1} \quad (7)$$

here, $A_{ul}$ is the Einstein coefficient for spontaneous emission, which for the Hα line is $7.94 \times 10^8$, $g_u$ is the statistical weight of the upper level, $g_u = 6$ (calculated from $g_u = 2J + 1$), where $J = 5/2$J, $N_e$ is the electron density in $cm^{-3}$, $E_u \approx \Delta E$ is the energy of the upper level, $E_u = 97\,492.36\ cm^{-1}$, $k_B$ is the Boltzmann

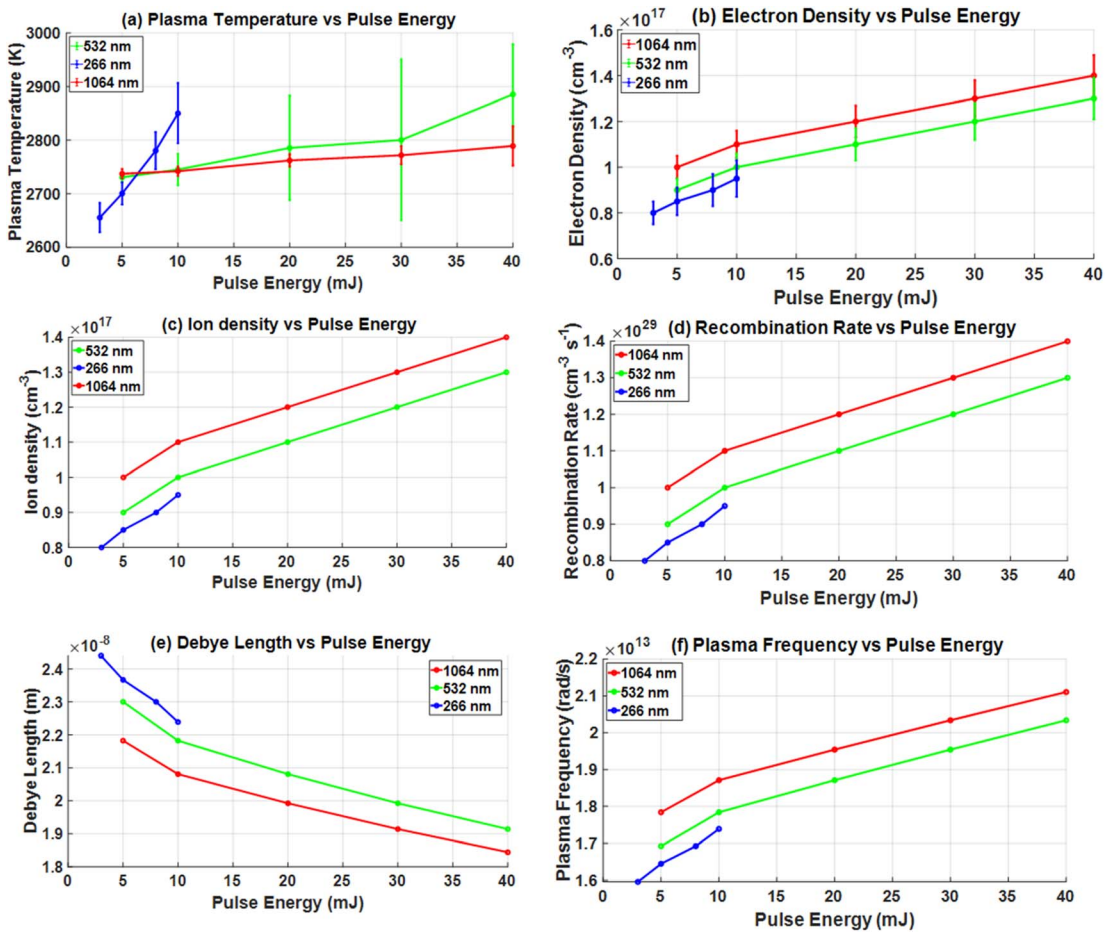


Fig. 8 Plasma parameters as a function of pulse energy: (a) temperature, (b) electron density, (c) ion density, (d) recombination rate, (e) Debye length, (f) and plasma frequency.

constant ($1.3 \times 10^{-23}$ J K$^{-1}$), $T$ is the plasma temperature in Kelvin. $\Delta\lambda_{1/2}$ is the full width at half maximum (FWHM). $2 \times 10^{-8}$ is the Stark broadening diagnostics in hydrogen plasma.

The recorded plasma temperatures, ranging from 2500 to 3000 K, correspond to thermal energies between 0.22 and 0.26 eV. The high-energy electrons and photons produced by plasma enhance the probability of bond breaking by photochemical and collisional mechanisms, even if the thermal energies are below the bond dissociation energies of C–C (~3.6 eV) and C–H (~4.3 eV). The fourth harmonic 266 nm laser beam releases photons with an energy of 4.66 eV, facilitating the direct cleavage of C–H bonds by single-photon absorption. The plasma temperatures indicated in the study are inadequate to disrupt chemical bonds *via* thermal excitation processes. The laser pulse produces focused energy and Hα line Stark broadening to increase electron density for electron impact dissociation and multiphoton absorption, which operate as alternate excitation pathways. The photonic and energetic environment of plasma significantly enhances the effectiveness of bond-breaking, especially for C–H bonds, beyond temperature effects alone. The plasma temperature and electron density produce thermal energy that induces molecular vibrations for fragment desorption, while energetic electrons and photons directly break chemical bonds. Experimental results indicate that the 266 nm laser generated more Hα emission and enhanced C–H bond dissociation due to its superior photon energy and plasma intensity relative to the 1064 nm and 532 nm laser excitations.

However, the temperature in this investigation is below the conventional LIBS experimental temperature range of 6000–10 000 K, possibly due to several different reasons. The limitations of our spectrometer (HR4000CG-UV-NIR) prevent the collection of delay-dependent data, resulting in an average temperature measurement of plasma instead of determining the peak temperature, since plasmas require delay-dependent measurements to identify peak temperatures, as these temperatures could reach several thousand or even tens of thousands of Kelvin but decrease rapidly after initial stimulation. The averaging process over time yields a measured result lower than the actual peak temperatures; moreover, low laser pulse energy, particularly at the 266 nm harmonic, and reliance on a singular Hα spectral line for temperature assessment. The assessment of plasma temperatures can be affected by partial self-absorption resulting from brief plasma lifetimes, low electron densities, dense core areas, and cooler outside zones, contributing to reabsorption phenomena.[40]

According to Fig. 8(a and b), the plasma diagnostics indicate a direct correlation between laser harmonic, pulse energy, and plasma temperature and electron density measurements. The Hα emission significantly increases during pulse energy elevations while employing fourth and second laser wavelengths, indicating considerable C–H bond dissociation because thermal and collisional mechanisms initiate the fragmentation of C–C bonds when the plasma temperature increases gradually and sustains electron concentrations. The fourth laser harmonic induces photonic effects since its photon energy of 4.66 eV exceeds the dissociation energies of 3.6 eV and 4.2 eV for both C–H and C–C bonds, respectively, since plasma formation in hydrogen-containing polymers employs thermal and photochemical processes to break chemical bonds.

Additional plasma parameters – ion density, recombination rate, Debye length, plasma frequency, and collision frequency – were obtained to get possible information to facilitate laser-induced HDPE pyrolysis and support the argument about the breaking of laser-induced HDPE bonds.

$$\text{Ion Density} = N_i = \frac{N_e}{N_{total} + N_e} N_{total} \quad (8)$$

$$\text{Recombination rate} = R = \alpha_r \times N_e \times N_i \quad (9)$$

$$\text{Plasma Frequency} = \lambda_D \sqrt{\frac{N_e \times e^2}{\varepsilon_0 \times m_e}} \quad (10)$$

The deficiency of data necessitated the formulation of certain parameter assumptions to derive information from the referenced eqn (8)–(10). The summary of utilized fundamental and reasonable assumed values is reported in Table 4. The computation of plasma characteristics, such as ion density, recombination rate, Debye length, plasma frequency, and collision frequency, necessitated a synthesis of recognized physical constants and context-specific, reasonable assumptions concerning laser-induced hydrogen plasma. The fundamental constants, including free space permittivity ($\varepsilon_0$), elementary charge ($e$), Boltzmann constant ($k$), and electron mass ($m_e$), function as precise numerical values that control electrostatic effects, charge motion, and the thermal behavior of electrons following established plasma physics models. A standard value for weakly associated plasmas is the Coulomb

Table 4 The parameter ranges used to calculate the additional plasma parameters

| Parameters | Symbol | Value | Description | References |
|---|---|---|---|---|
| Coulomb logarithm | $\ln \Lambda$ | 15 | Typical value for weakly coupled plasmas | 41 |
| Recombination coefficient | $\alpha_r$ | $1 \times 10^{-13}$ cm$^3$ s$^{-1}$ | Assumed value | 42 |
| Total number density | $N_{Total}$ | $1 \times 10^{19}$ cm$^{-3}$ | Density of hydrogen atoms | 43 |
| The permittivity of free space | $\varepsilon_0$ | $8.854 \times 10^{-12}$ F m$^{-1}$ | Physical constant | 44 |
| Elementary charge | $e$ | $1.602 \times 10^{-19}$ C | Fundamental constant | 45 |
| Boltzmann constant | $k$ | $1.380 \times 10^{-23}$ J K$^{-1}$ | Fundamental constant | 46 |
| Electron mass | $m_e$ | $9.109 \times 10^{-31}$ kg | Fundamental constant | 46 |

logarithm ($\ln \Lambda = 15$), indicating the predominance of small-angle scattering due to the low-density, high-temperature conditions of the system.[41] This selection corresponded with literature ranges of 10–20 for analogous situations. The recombination coefficient ($\alpha_r$) was derived using standard radiative recombination rates of H plasmas at temperatures of about $10^4$ K, remaining within the range of $10^{-13}$ to $10^{-12}$ cm$^3$ s$^{-1}$.[42] The total number density ($N_{Total}$) indicates the neutral hydrogen background, an appropriate indicator for plasmas partially ionized by pulsed lasers since investigations reveal neutral hydrogen densities ranging from $10^{18}$ to $10^{20}$ cm$^{-3}$. The aggregated selection of parameters yields physically significant outputs that characterize experimental plasma conditions and include numerous experimental inputs. The study's values must derive from empirical facts rather than being arbitrary. Identifying data from H-rich plasma represents the initial step of this approach.

Fig. 8(a) and (b) illustrate the correlation between plasma temperature and electron density of HDPE as a function of pulse energy. Notably, the fourth harmonic demonstrated consistent efficiency across all instances, as reflected by the observed electron density and changes in plasma temperature. The fourth harmonic, particularly effective at generating higher plasma temperatures, exhibits exceptional performance in HDPE bond cleavage due to a continuum in the emission spectrum. This continuum facilitates enhanced energy transfer and forms a dense plasma within the HDPE. The plasma temperature for the 266 nm harmonic reaches approximately 2800 K at 10 mJ, significantly surpassing the 2700 K observed in the first and second harmonics, even at higher pulse energies. The continuous emission indicates the release of a broad spectrum of wavelengths, aligning with high-energy electron-ion collisions in the plasma. This increases plasma temperature, which enhances the efficiency of breaking C–C and C–H bonds in HDPE. While the pronounced continuum and elevated plasma temperature may not be ideal for electron densities, they create an optimal environment for bond cleavage, reducing potential damage to the HDPE. In contrast, the first and second harmonics, despite generating higher electron densities, produce plasma conditions that are less efficient for HDPE bond cleavage. Due to its higher plasma temperatures and lower electron densities, the continuum in the fourth harmonic spectrum makes it the most effective laser harmonic for efficiently breaking HDPE bonds.

Fig. 8(c–f) depict significant plasma details associated with the dissociation of HDPE bonds during laser ablation at various wavelengths (266 nm, 532 nm, and 1064 nm). Fig. 8(c) illustrates that ion density increases with pulse energy across all wavelengths, with the most significant effect observed at 1064 nm, signifying enhanced ionization. Fig. 8(d) indicates that recombination rates increase around 1064 nm, implying that ionized particles rapidly revert to a neutral state, reducing the energy available for bond dissociation. Fig. 8(e) illustrates a reduction in Debye length with increasing pulse energy, especially at extended wavelengths, signifying a more concentrated plasma environment. However, the plasma frequency reveals a higher rate for shorter wavelengths than other harmonics, as illustrated in Fig. 8(f). Conversely, 266 nm has reduced recombination and a higher frequency rate, rendering it more efficient for cleaving HDPE bonds. While longer wavelengths produce higher plasma, their efficiency is reduced because of increased energy loss from collisions and recombination. Consequently, 266 nm is the optimum laser wavelength for HDPE bond dissociation since it reduces energy dissipation and concentrates the absorbed energy more efficiently on breaking the chemical bonds.

### 4.4. Microscopic analysis

All the ablated HDPE samples and optical microscopic view can be found in the ESI (Fig. 10 and 11);† however, the higher pulse energies, such as 40 mJ for the first and second harmonic and 10 mJ for the fourth harmonic, can be found in Fig. 9 with 50 times magnified view. The top row in Fig. 9 shows the laser-ablated HDPE samples, while the bottom row presents the reflected microscopic views of the ablated areas to illustrate melting, damage, and crater formation as a function of laser harmonics. The sample was rotated at a speed of 240 degrees per second, completing a full 360-degree rotation for the collection of 30 shots of data. To prevent damage to the sample and maintain spectral consistency, it was rotated at 48 degrees per second using a motorized stage. This spin functioned independently from the laser pulses, just preventing the laser from striking the identical location repeatedly. The quick scanning, with each pulse emitted every 50 ms, reduced overheating, cratering, and inconsistent data capture in the same region. The method ensured a homogeneous surface, enhancing the reliability of the LIBS signal without the need for a synchronization device. The existing equipment has a maximum attainable rotation angle, which will be enhanced in future trials. To conduct a more comprehensive analysis, the sample that had undergone ablation was examined using an optical microscope equipped with lenses that provided 50× magnification.

The laser ablation of HDPE exhibited distinct variations across the first, second, and fourth harmonics. The first harmonic, even at higher energy levels (up to 40 mJ), demonstrated a more localized impact with substantial material removal, whereas the second harmonic induced extensive and connected material loss at comparable energies, as shown in Fig. 9. In contrast, the fourth harmonic displayed precise bond breaking and controlled material removal, with minimal surface damage, even at lower energy levels (3–5 mJ). As energy increased (8–10 mJ), the fourth harmonic caused significant surface alterations, including crater formation, melting, and material deformation. Notably, the second harmonic's shorter wavelength and higher photon energy enabled more efficient bond breaking, whereas the fourth harmonic's UV region light directly broke bonds, facilitated by multiphoton absorption. These findings underscore the importance of laser harmonic selection and energy level optimization for tailored bond-breaking processes in HDPE. According to Fig. 9, microscopic examination reveals that the fourth laser harmonic at 266 nm is optimal for HDPE bond breaking, particularly C–H bond

 

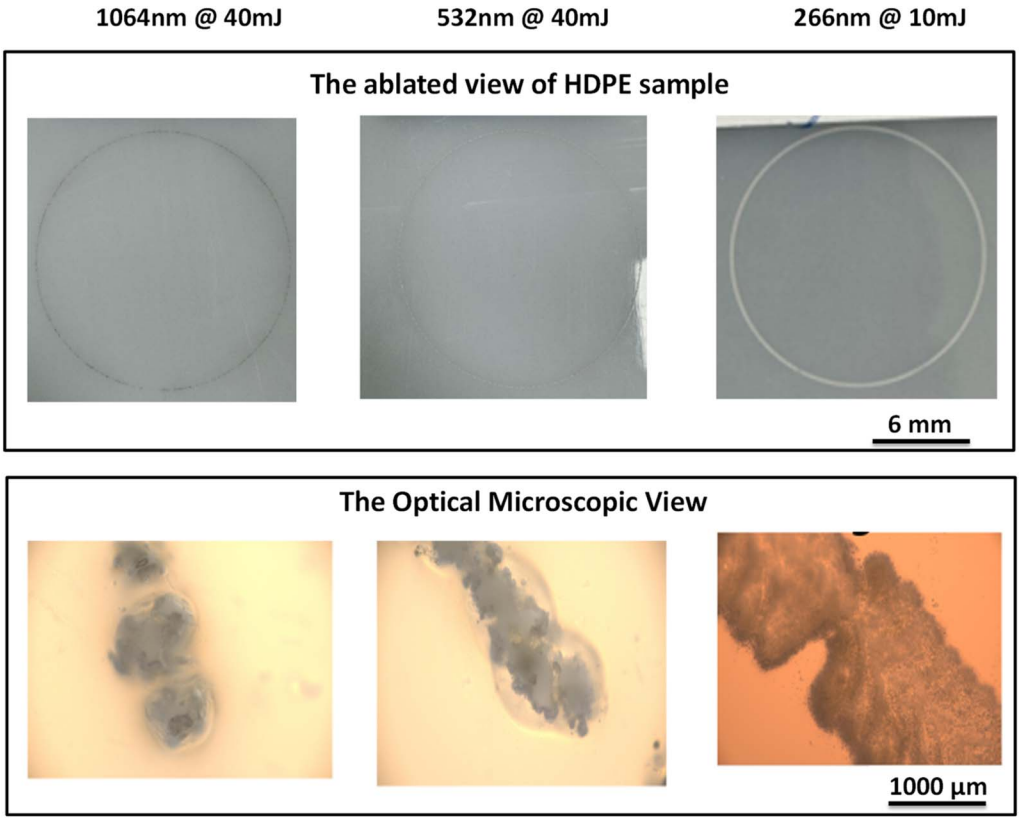


Fig. 9 The ablated HDPE samples and optical microscopic view presented at the micrometre scale of HDPE sample at higher pulse energies are shown for (left) the first harmonic, (middle) the second harmonic, and (right) the fourth harmonic.

dissociation, due to its ability to achieve minimal sample ablation and precise bond-breaking.

### 4.5. Limitation and future perspective

This study utilized a non-gated spectrometer to acquire spectra, with integration durations optimized *via* time scans to suppress background interference and enhance signal quality. While the absence of time-resolved gating may pose limitations, multiple analytical approaches such as peak fitting, baseline correction, and background subtraction were employed to isolate discrete emission signals. Notably, spectral lines for C–C, C–H, and Hα were consistently detected across laser harmonics (1064 nm, 532 nm, and 266 nm), confirming their material origin rather than instrumental artefacts. The correlation between Hα intensity fluctuations at 266 nm and documented bond dissociation energies underscores the validity of these signals, aligning with photonic energy principles.

Integration strategies minimized early-stage bremsstrahlung continuum emissions during plasma cooling (2500–3000 K). Although these plasma regimes occasionally deviated from Local Thermodynamic Equilibrium (LTE), spectral lines with analogous excitation potentials were prioritized, avoiding those prone to optical thickness or self-absorption. Symmetrical emission line geometries further indicated negligible reabsorption effects. While absolute plasma temperatures were lower than conventional time-gated LIBS regimes (~6000–10 000 K), consistent relative wavelength patterns across laser parameters reinforced the reliability of bond-specific conclusions. The observed Hα intensity variations corroborate HDPE's wavelength-dependent dissociation theory, affirming the persistence of photonic energy effects under diverse experimental conditions. Future work will incorporate gated ICCD detection and a digital delay generator to enable time-resolved plasma diagnostics, improving signal discrimination and quantitative precision.

## 5. Analytical discussion

The findings on the bond-breaking process in HDPE introduce several critical considerations. The selection of low-intensity process parameters for breaking C–C and C–H bonds was a deliberate choice to balance efficiency and minimize thermal damage. Although higher pulse energy could theoretically accelerate bond dissociation, it also increases the risk of excessive thermal degradation, complicating analysis. Excessive energy input could significantly increase fluorescence intensity, sample weight loss, and the possible formation of hazardous gases such as cyanide. The reported literature does not provide definitive threshold energy values for HDPE bond dissociation using different laser harmonics. While this study employed three laser harmonics spanning from UV to NIR, it is essential to recognize that different harmonics may require distinct

energy thresholds for effective direct and indirect bond breaking. The direct and indirect bond breaking refers to the energy of each laser harmonic's photons. For example, the first and second harmonics correspond to photon energies of 1.17 eV and 2.3 eV, below the dissociation energies of the C–C and C–H bonds (3.6 eV and 4.2 eV, respectively). Therefore, it is reasonable to claim that photons do not directly break the bonds. However, the emission intensities verify that bond breaking is attributed to indirect mechanisms, such as multi-photon absorption, which can lead to cascade phenomena and photothermal and photochemical reactions that facilitate bond breaking. Similarly, in the case of the fourth harmonic laser, with a single photon energy of 4.65 eV, it is sufficient to break the bonds directly due to the energetic photons. Additional mechanisms, such as photothermal and photochemical bond-breaking, can further facilitate the breaking and initiate reactions. Therefore, it is logical and reasonable to claim that the first and second laser harmonics broke the bonds indirectly, while the fourth harmonic broke the bonds directly through photons.

Additionally, based on the spectrum obtained from the fourth laser harmonic, it can be reasonably claimed that it effectively breaks C–H bonds. This is because the photons in the UV region excite H-atoms, and the C–H bonds absorb energy at this wavelength due to their excitation levels, which could promote bond-breaking through resonance effects. The emission spectra from the fourth harmonic show H-emission at 656.3 nm, with an intensity twice as strong as the C–C emission and higher than all other harmonics. This increased H-emission intensity further supports the notion that the fourth harmonic is more efficient at breaking C–H bonds than other harmonics. Spectral intensity studies also indicate that the fourth harmonic is particularly effective. Without solid evidence, it is still a hypothesis that the fourth laser harmonics facilitate more C–H breaking, which will be verified in future investigations. The absence of UV laser applications directly breaking these bonds, highlights a research gap requiring further investigation. Multiphoton absorption enables different laser harmonics to effectively dissociate HDPE bonds, reinforcing the rationale for using minimal pulse energy to prevent unnecessary degradation. The structural complexity of HDPE, with its long-chain branched configuration, adds another difficulty in determining the energy threshold for breaking all bonds. The distinction between bond cleavage in small *versus* large branches remains unclear, as these events occur on the picosecond to femtosecond timescale, complicating real-time analysis. While the minimum energy required for breaking C–C and C–H bonds has been established, the precise sequence in which bonds within branched structures break demands further empirical validation.

The energy requirements for bond dissociation may vary based on bond proximity and interaction dynamics. The HDPE sample was rotated during laser exposure to mitigate potential damage and maintain consistent signal acquisition. Without rotation, continuous photon bombardment on a fixed location could lead to nonlinear absorption effects, adversely impacting the results. A rotation speed of 48 degrees per second, dictated by the sample holder's design, facilitated data collection from 150 distinct laser pulses, enhancing data integrity by capturing signals from multiple surface areas. However, as observed in spectroscopic analysis, numerous photons can interact with the exact location. This phenomenon could either enhance reaction rates or reduce signal intensity depending on the interaction conditions. While this aspect requires further investigation, it presents intriguing implications for optimizing laser-induced pyrolysis and improving hydrocarbon breakdown efficiency. These findings underscore the innovative intersection of laser technology and polymer science, challenging the notion that laser-induced HDPE breakdown is impractical. The results of this study provide empirical support for this process, opening new pathways for understanding bond behavior and enhancing plastic recycling techniques. Insights into the fourth laser harmonic's interaction with HDPE, including the threshold energy required to initiate reactions, offer contributions to optimizing laser-induced HDPE pyrolysis. So far, none of the cited literature on lasers has addressed the role of bond breaking under different experimental and environmental conditions, the formation routes, and the potential combination of laser harmonics with other approaches to develop a hybrid methodology. The primary focus has been identifying elements, categorizing types, utilizing machine learning, and recognizing distinctive plastics, resulting in exceptional performance and significant insights. For instance, the research carried out in the last five years demonstrates the limitations of LIBS in the context of plastic recycling. Nevertheless, the question persists: Why, despite extensive research, is economically viable plastic recycling not yet taking place? The main difficulty of the issue lies in understanding the breakdown of plastic bonds, the resulting reactions, and the subsequent responses. Without this knowledge, achieving sustainability in plastic recycling is unattainable. A comprehensive investigation has been conducted in response to these challenges, revealing numerous novel insights and presenting significant information.

## 6. Conclusion

This experimental study confirms our claim about laser-induced HDPE pyrolysis since it has been demonstrated that different laser harmonics can effectively break HDPE bonds even with the photon energy lower than the C–C and C–H dissociation threshold. This investigation provides a deep insight into the bond-breaking mechanism, such as the impacts of multiphoton interactions, the absorption process, and threshold determination, that can support laser-induced HDPE pyrolysis. The fourth laser harmonic exhibits high efficiency in breaking HDPE bonds, particularly C–H bonds, due to the UV region photons; C–H bonds absorb this energy due to their excited states, where C–H bond breaking may be attributed to the resonance effects. However, it is challenging to claim this time that the Hα intensity was potentially relevant to breaking parent or daughter atoms, perhaps both. The optical microscopic analysis demonstrates the low surface ablation of HDPE with the fourth laser harmonic, which can promote the

reduction in thermal effect and facilitate selective bond breaking. The detail associated with the energy threshold required to initiate the reaction, the behavior of bonds under the different laser harmonic, the influence of experimental process parameters, the comprehension of the ablation mechanism, $R^2$ value of 0.9758, rising electron density and plasma temperature of 2800 K, could offer valuable insights for advancing laser-induced HDPE pyrolysis. It is reasonable to assume that there is something curious about the behaviour of HDPE bonds and the laser harmonic impacts in a vacuum are needed to gain insight into the product formation routes.

## Data availability

The data supporting the findings of this study are available from the corresponding author upon reasonable request.

## Conflicts of interest

There are no conflit of interest.

## Acknowledgements

This work was in part supported by the Shanghai Science and Technology Program (Grant No. 21511105000), NSAF (Grant No. U2130123), and the International Partnership Program of the Chinese Academy of Sciences (Grant No. 181231KYSB20200033). Rao Adeel Un Nabi acknowledges the Chinese Scholarship Council for International Students.

## References

1 R. A. U. Nabi, H. A. Khawaja, Y. X. Liu, C. Yang, J. Long, X. Li and T. J. Wang, A hypothetical approach toward laser-induced high-density polyethylene pyrolysis, *Sustainable Mater. Technol.*, 2024, e01074, DOI: 10.1016/j.susmat.2024.e01074.

2 Y. Wan, Q. Zeng, P. Shi, Y. J. Yoon, C. Y. Tay and J. M. Lee, Machine learning-assisted optimization of TBBPA-bis-(2, 3-dibromopropyl ether) extraction process from ABS polymer, *Chemosphere*, 2022, **287**, 132128, DOI: 10.1016/j.chemosphere.2021.132128.

3 Y. Wan, Q. Zeng, P. Shi, Y. J. Yoon, C. Y. Tay and J. M. Lee, Machine learning-assisted optimization of TBBPA-bis-(2, 3-dibromopropyl ether) extraction process from ABS polymer, *Chemosphere*, 2022, **287**, 132128, DOI: 10.1016/j.chemosphere.2021.132128.

4 C. Jia, P. Das, I. Kim, Y. J. Yoon, C. Y. Tay and J. M. Lee, Applications, treatments, and reuse of plastics from electrical and electronic equipment, *J. Ind. Eng. Chem.*, 2022, **110**, 84–99, DOI: 10.1016/j.jiec.2022.03.026.

5 R. Zuo, Y. Xiong, J. Wang and E. J. M. Carranza, Deep learning and its application in geochemical mapping, *Earth-Sci. Rev.*, 2019, **192**, 1–14, DOI: 10.1016/j.earscirev.2019.02.023.

6 T. Chen, T. Zhang and H. Li, Applications of laser-induced breakdown spectroscopy (LIBS) combined with machine learning in geochemical and environmental resources exploration, *TrAC, Trends Anal. Chem.*, 2020, **133**, 116113, DOI: 10.1016/j.trac.2020.116113.

7 *Laser Spectroscopy of Atoms and Molecules*, ed. H. Walther, Springer, 2006, vol. 2, DOI: 10.1007/978-3-030-73893-8.

8 Q. Zeng, J. B. Sirven, J. C. P. Gabriel, C. Y. Tay and J. M. Lee, Laser induced breakdown spectroscopy for plastic analysis, *TrAC, Trends Anal. Chem.*, 2021, **140**, 116280, DOI: 10.1016/j.trac.2021.116280.

9 R. Junjuri, A. P. Gummadi and M. K. Gundawar, EXPRESS: Standoff Identification of Plastic Waste Using a Low-Cost Compact Laser-Induced Breakdown Spectroscopy LIBS Detection System, *Appl. Spectrosc.*, 2024, **78**, 1089, DOI: 10.1177/00037028241268348.

10 L. Brunnbauer, M. Jirku, C. D. Quarles Jr and A. Limbeck, Capabilities of simultaneous 193 nm-LIBS/LA-ICP-MS imaging for microplastics characterization, *Talanta*, 2024, **269**, 125500, DOI: 10.1016/j.talanta.2023.125500.

11 G. Bonifazi, G. Capobianco, P. Cucuzza, S. Serranti and V. Spizzichino, Black plastic waste classification by laser-induced fluorescence technique combined with machine learning approaches, *Waste Biomass Valoriz.*, 2024, **15**(3), 1641–1652, DOI: 10.1007/s12649-023-02146-z.

12 C. Lubongo, M. A. A. Bin Daej and P. Alexandridis, Recent Developments in Technology for Sorting Plastic for Recycling: The Emergence of Artificial Intelligence and the Rise of the Robots, *Recycling*, 2024, **9**(4), 59, DOI: 10.3390/recycling9040059.

13 J. Yang, Y. P. Xu, P. Chen, J. Y. Li, D. Liu and X. L. Chu, Combining spectroscopy and machine learning for rapid identification of plastic waste: recent developments and future prospects, *J. Clean. Prod.*, 2023, **431**, 139771, DOI: 10.1016/j.jclepro.2023.139771.

14 E. R. K. Neo, J. S. C. Low, V. Goodship, S. R. Coles and K. Debattista, Development of a polymer spectral database for advanced chemometric analysis, *Procedia*, 2023, **116**, 197–202, DOI: 10.1016/j.procir.2023.02.034.

15 J. Shen, J. Dai, H. Lin, S. Li, S. Gao, Y. Cheng, M. Patrascu and X. Gao, Multiscale Modeling of Plastic Pyrolysis with a Neural Network-Inspired Pyrolysis Kinetic Model and Coarse-Grained DEM-CFD, *Ind. Eng. Chem. Res.*, 2024, **63**(28), 12688–12703, DOI: 10.1021/acs.iecr.4c01882.

16 H. Heriyanto, E. Suhendi, M. Y. Nasheh, M. F. Rizqillah, W. Wardalia and H. Pujiastuti, The Influence of NaturalBayah Zeolite on the Pyrolysis Process of Liquid Fuel Based on HDPE and P.P. Plastic Waste, *World Chem. Eng. J.*, 2024, **8**(1), 26–33, DOI: 10.36055/wcej.v8i1.26617.

17 K. Manickavelan, S. Sivaganesan, M. V. Kulkarni and S. Sivamani, Response surface design, modelling and analysis on pyrolysis of waste high-density polyethylene (HDPE), *J. Mater. Cycles Waste Manage.*, 2024, **26**(1), 491–500, DOI: 10.1007/s10163-023-01846-x.

18 A. C. Aydogdu, B. Erkmen, A. Suerkan, A. Ezdesir, B. Guliyev and G. Celik, Chemical upcycling of polyolefins into liquid refinery feedstock from the circularity and chemical engineering aspects, *J. Environ. Chem. Eng.*, 2024, **12**(5), 113430, DOI: 10.1016/j.jece.2024.113430.

19 P. Das, P. Tiwari and J. M. Lee, Multistep kinetic analysis of additive-enhanced plastic degradation, *Chem. Eng. J.*, 2024, **488**, 150960, DOI: 10.1016/j.cej.2024.150960.
20 P. Shi, T. Huang, H. K. Lim, C. K. Tan, J. M. Lee and C. Y. Tay, Transforming electronic plastics into bioadaptive 3D porous construct for advanced cell culture applications, *Resour., Conserv. Recycl.*, 2024, **200**, 107297, DOI: 10.1016/j.resconrec.2023.107297.
21 P. Das, J. C. P. Gabriel, C. Y. Tay and J. M. Lee, Value-added products from thermochemical treatments of contaminated e-waste plastics, *Chemosphere*, 2021, **269**, 129409, DOI: 10.1016/j.chemosphere.2020.129409.
22 R. A. U. Nabi, M. Y. Naz, S. Shukrullah and A. Ghaffar, A Critical Review on Waste Plastic into Value-Added Hydrocarbons and Fuels, *Energy Environ. Tropics*, 2022, 145–156, DOI: 10.1007/978-981-19-6688-0_9.
23 P. Shi, Y. Wan, A. Grandjean, J. M. Lee and C. Y. Tay, Clarifying the in-situ cytotoxic potential of electronic waste plastics, *Chemosphere*, 2021, **269**, 128719, DOI: 10.1016/j.chemosphere.2020.128719.
24 A. P. Michel, A. E. Morrison, V. L. Preston, C. T. Marx, B. C. Colson and H. K. White, Rapid identification of marine plastic debris via spectroscopic techniques and machine learning classifiers, *Environ. Sci. Technol.*, 2020, **54**(17), 10630–10637, DOI: 10.1021/acs.est.0c02099.
25 W. Cao, Y. Li, B. Yan, Z. Zeng, P. Liu, R. Li, J. Jiang, Z. Ke and G. Yang, Catalyst-Free Activation and Fixation of Nitrogen by Laser-Induced Conversion, *J. Am. Chem. Soc.*, 2024, **146**, 14765, DOI: 10.1021/jacs.4c02631.
26 A. Kushwaha and R. K. Thareja, Dynamics of laser-ablated carbon plasma: formation of C2 and CN, *Appl. Opt.*, 2008, **47**(31), G65–G71, DOI: 10.1364/ao.47.000g65.
27 R. S. Ram and P. F. Bernath, Fourier transform emission spectroscopy of the A2Π–X2Σ+(red) system of 13C14N (II), *J. Mol. Spectrosc.*, 2012, **274**, 22–27, DOI: 10.1016/j.jms.2012.03.008.
28 P. Das, Q. Zeng, A. Leybros, J. C. P. Gabriel, C. Y. Tay and J. M. Lee, Enhanced extraction of brominated flame retardants from e-waste plastics, *Chem. Eng. J.*, 2023, **469**, 144126, DOI: 10.1016/j.cej.2023.144126.
29 P. Wangchingchai, M. Karino, K. Yamasaki and H. Kohguchi, N–H and N–C Bond Dissociation Pathways in Ultraviolet Photodissociation of Dimethylamine, *J. Phys. Chem. A*, 2024, **128**(10), 1871–1879, DOI: 10.1021/acs.jpca.4c00001.
30 H. K. Eidesen, H. Khawaja and S. Jackson, Simulation of the HDPE Pyrolysis Process, *Int. J. Multiphys.*, 2018, **12**, 79.
31 R. A. U. Nabi, M. Y. Naz, S. Shukrullah, M. Ghamkhar, N. U. Rehman, M. Irfan, A. O. Alqarni, S. Legutko, I. Kruszelnicka, D. Ginter-Kramarczyk and M. Ochowiak, Analysis of statistically predicted rate constants for pyrolysis of high-density plastic using R software, *Materials*, 2022, **15**(17), 5910, DOI: 10.3390/ma15175910.
32 J. E. Mark, *Physical Properties of Polymers Handbook*, ed. J. E. Mark, Springer, New York, 2007, vol. 1076. DOI: DOI: 10.1007/978-0-387-69002-5.
33 A. C. Walker, T. Stamatakis and I. J. Spalding, The heating of polyethylene pellets with kilojoule, microsecond duration, CO2 laser pulses, *J. Phys. D: Appl. Phys.*, 1978, **11**(16), 2285, DOI: 10.1088/0022-3727/11/16/016.
34 A. O. Alqarni, R. A. U. Nabi, F. Althobiani, M. Y. Naz, S. Shukrullah, H. A. Khawaja, M. A. Bou-Rabee, M. E. Gommosani, H. Abdushkour, M. Irfan and M. H. Mahnashi, Statistical optimization of pyrolysis process for thermal destruction of plastic waste based on temperature-dependent activation energies and pre-exponential factors, *Processes*, 2022, **10**(8), 1559, DOI: 10.3390/pr10081559.
35 M. Irfan, R. A. U. Nabi, H. Hussain, M. Y. Naz, S. Shukrullah, H. A. Khawaja, S. Rahman and M. U. Farid, Statistical prediction and sensitivity analysis of kinetic rate constants for efficient thermal valorization of plastic waste into combustible oil and gases, *Heliyon*, 2023, **9**(5), e16049, DOI: 10.1016/j.heliyon.2023.e16049.
36 M. Irfan, R. A. U. Nabi, H. Hussain, M. Y. Naz, S. Shukrullah, H. A. Khawaja, S. Rahman and F. Althobiani, Numerical sensitivity analysis of temperature-dependent reaction rate constants for optimized thermal conversion of high-density plastic waste into combustible fuels, *Can. J. Chem. Eng.*, 2023, **101**(10), 5611–5620, DOI: 10.1002/cjce.24883.
37 F. Yin, T. J. Wang, Y. Liu, J. Long, Y. Wei, B. Zhu, K. Zhou and Y. Leng, Pulse repetition rate effect on the plasma inside femtosecond laser filament in air, *Chin. Opt. Lett.*, 2024, **22**, 013201, DOI: 10.3788/COL202422.013201.
38 J. V. Foltz, D. H. Rank and T. A. Wiggins, Determinations of some hydrogen molecular constants, *J. Mol. Spectrosc.*, 1966, **21**(1–4), 203–216, DOI: 10.1016/0022-2852(66)90138-X.
39 R. A. U. Nabi, H. A. Khawaja, Y. Xiangliu, C. Yang, R. ul Haq and T.-J. Wang, Laser-Induced Plasma Effects on Bond Breaking in High-Density Polyethylene Pyrolysis, *Adv. Mater. Interfaces*, 2025, 2500138, DOI: 10.1002/admi.202500138.
40 T. Baeva, High Harmonic Generation from Relativistic Plasma, PhD thesis, 2008, , DOI: 10.48550/arXiv.physics/0604228.
41 M. A. Martínez-Fuentes, C. Sánchez-Aké, J. J. E. Herrera-Velázquez and M. Villagrán-Muniz, Complementary characterization of laser-induced plasmas by optical emission spectroscopy and triple langmuir probe, *IEEE Trans. Plasma Sci.*, 2019, **47**(12), 5299–5305, DOI: 10.1109/TPS.2019.2951392.
42 I. Saxena, K. Ehmann and J. Cao, A Comparative Study of Laser Induced Plasma Micro-Machining and Laser Ablation of Low Melting Point Polymers, *Int. Workshop Microfactories*, 2014, pp. 290–295, DOI: 10.1115/MSEC2010-34242.
43 C. S. Costa, A. Fernandes, M. Munoz, M. R. Ribeiro and J. M. Silva, Analyzing HDPE Thermal and Catalytic Degradation in Hydrogen Atmosphere: A Model-Free Approach to the Activation Energy, *Catalysts*, 2024, **14**(8), 514, DOI: 10.3390/catal14080514.
44 S. Bagchi and D. Perez, Atomistic modeling of the coupling between electric field and bulk plastic deformation in fcc

metals, *Phys. Rev. Accel. Beams*, 2022, **25**(3), 033101, DOI: **10.1103/PhysRevAccelBeams.25.033101**.

45 J. Y. Cui, T. T. Li, Z. H. Yin, L. Chen and J. J. Wang, Remarkably enhanced acidic photoelectrochemical glycerol oxidation achievingthe theoretical maximum photocurrent of BiVO4 through anion modulation, *Chem. Eng. J.*, 2024, **493**, 152461, DOI: **10.1016/j.cej.2024.152461**.

46 R. Liotard, B. Canaud, A. Pineau, A. Sollier, E. Lescoute, A. Colaço, S. Bouklah and M. Etourneau, Heterogeneous catalytic effect of perovskite oxide–based electrodes for efficient energy storage, *J. Appl. Electrochem.*, 2023, **53**(10), 1143–1152, DOI: **10.1007/s10800-023-01645-x**.